

Constrained Acquisition of Ink Spreading Curves from Printed Color Images

Thomas Bugnon, and Roger D. Hersch, *Member, IEEE*

Abstract— Today’s spectral reflection prediction models are able to predict the reflection spectra of printed color images with an accuracy as high as the reproduction variability allows. However, to calibrate such models, special uniform calibration patches need to be printed. These calibration patches use space and have to be removed from the final product. The present contribution shows how to deduce the ink spreading behavior of the color halftones from spectral reflectances acquired within printed color images. Image tiles of a color as uniform as possible are selected within the printed images. The ink spreading behavior is fitted by relying on the spectral reflectances of the selected image tiles. A relevance metric specifies the impact of each ink spreading curve on the selected image tiles. These relevance metrics are used to constrain the corresponding ink spreading curves. Experiments performed on an inkjet printer demonstrate that the new constraint-based calibration of the spectral reflection prediction model performs well when predicting color halftones significantly different from the selected image tiles. For some prints, the proposed image based model calibration is more accurate than a classical calibration.

Index Terms—Color prints, color reproduction, dot gain, halftones, ink spreading, prediction model calibration, spectral reflection prediction

I. INTRODUCTION

THE goal of a color reproduction device is to be able to reproduce input colors as accurately as possible. To achieve faithful color reproduction, devices must be both calibrated and characterized [1]. Device calibration ensures that the device has a known characteristic color response. Device characterization relates this characteristic color response to a device independent representation. Both device calibration and characterization can benefit from the use of a model predicting the reflectance of color halftones as a function of their nominal surface coverages, i.e. of the control values specifying the amount of inks to be printed. For device calibration, spectral reflection prediction models are helpful in studying the influence of given factors on the range of

printable colors: the inks, the type of paper, the illumination conditions, and the halftones. A spectral reflection prediction model is also useful for the characterization of a printing device since it predicts the device-independent color values resulting from a set of nominal ink surface coverages. It therefore enables the creation of ICC profiles for color management [2] as well as new color separation strategies, for example when printing with custom inks [3].

The present contribution focuses on the calibration of a model predicting the reflection spectra of color halftones printed on a specific printer. The considered spectral reflection prediction model used is the Yule-Nielsen spectral Neugebauer model extended to account for ink spreading [4][5]. Classical model calibration is performed by measuring the reflection spectra of specially printed calibration patches and by deducing the ink spreading functions mapping nominal ink surface coverages to effective ink surface coverages. These special calibration patches comprise all solid colorants (paper, solid inks and solid ink superpositions) and single ink halftones superposed with all combinations of solid ink superpositions. However, these specially conceived calibration patches take valuable space on the printed product and must be removed. For example, on offset presses, the special calibration patches are placed in the margins of the printed pages and are cut off before assembling the final print product.

By deducing the ink spreading curves from chosen image tiles located within printed color images, we eliminate the need of printing special halftone calibration patches. However, some image tiles may not be relevant for determining certain ink spreading curves. To prevent the calibration procedure from setting these ink spreading curves to artificially large values, we impose additional constraints on the calibration procedure which rely on a relevance metric. We compare the predictions of the new model calibrations to the predictions of the classical calibrations. Thanks to the new calibration, the model predicts not only image tiles similar to the calibration tiles, but also uniform patches spanning the entire printing gamut. Moreover, the new predictions are in some cases more accurate than classical predictions, suggesting that the patches used for classical calibrations may not be the most relevant patches for model calibration.

Note that all the experiments have been performed on an inkjet printer, i.e. a device that provides a stable reproduction of colors across the entire page as well as from page to page. These assumptions are not valid for all reproduction devices.

Manuscript received April xx, 2009.

T. Bugnon and R. D. Hersch are with the École Polytechnique Fédérale de Lausanne (EPFL), 1015 Lausanne, Switzerland.

Published Item Identifier xxx

For example, in offset printing, the printable area is divided into several inking zones perpendicular to the printing direction. The ink flow is specific to each zone and depends on the amount of ink used within that zone. Ink spreading may therefore vary from zone to zone. The study of zone-dependent reproduction systems is out of the scope of the present paper.

The remainder of this paper is organized as follows. Section II introduces the Yule-Nielsen modified Spectral Neugebauer model (YNSN). Section III details the ink spreading model as well as the characterization of the ink spreading curves. The extended Yule-Nielsen modified Spectral Neugebauer model (IS-YNSN), which incorporates the ink spreading model, is introduced in Section IV. Section V details the problems related to calibrating the ink spreading model using reflectance spectra acquired from printed color image tiles. A new model calibration method is proposed which relies on a metric evaluating the relevance of each ink spreading curve for a given set of color image tiles. In Section VI, we describe the selection of image tiles of a color as uniform as possible for the calibration of the ink spreading model and for the tests of the prediction accuracy. The experimental setup is described in Section VII. The experiments and the resulting calibrated ink spreading curves are described in Section VIII. We discuss the prediction accuracy of the different calibration approaches in Section IX. The conclusions are drawn in Section X.

II. THE YULE-NIELSEN MODIFIED SPECTRAL NEUGEBAUER MODEL (YNSN)

One of the first color prediction models is the Neugebauer model [6]. In its original form, it predicts the CIE-XYZ tristimulus values of a color halftone patch as the sum of the tristimulus values of their individual colorants weighted by their fractional area coverages a_i . By considering the reflection spectra R_i of colorants instead of their respective tri-stimulus values, one obtains the spectral Neugebauer equations [7]. They predict the reflection spectrum of a printed color halftone patch as a function of the reflection spectra of its individual colorants (also called Neugebauer primaries):

$$R(\lambda) = \sum_i a_i * R_i(\lambda) \quad (1)$$

With k inks, there are 2^k colorants: white, the k single ink colorants and all the different superpositions of solid inks. For example, the red colorant is the superposition of the magenta

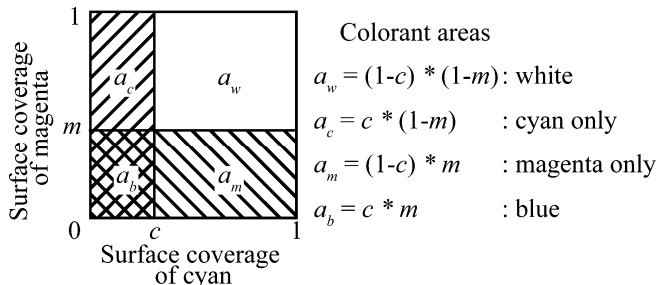


Fig. 1. Demichel equations giving the surface coverages of the four colorants created by the superposition of 2 inks of surface coverages c and m .

and yellow inks. When the ink layers are printed independently one from another, the fractional area coverages of the individual colorants are calculated from the surface coverages of the inks by the Demichel equations [2]. These equations are shown in Fig. 1 for the case of 2 inks, but can be extended to accommodate three or four inks (see Appendix B for the extension to 4 inks).

Since the Neugebauer model neither takes explicitly into account the lateral propagation of light within the paper bulk nor the internal reflections (Fresnel reflections) at the paper-air interface, its predictions are not accurate [8]. Yule and Nielsen [9] modeled the non-linear relationship between the reflectances of paper, single ink halftones, and the corresponding solid ink prints by a power function whose exponent n can be optimized according to the reflectances of a limited set of halftone patches. Viggiano [7] applied the Yule-Nielsen relationship to the spectral Neugebauer equations, yielding the Yule-Nielsen modified Spectral Neugebauer model (YNSN):

$$R(\lambda) = \left(\sum_i a_i * R_i(\lambda)^{1/n} \right)^n \quad (2)$$

Knowing the reflection spectra of the colorants R_i and the Yule-Nielsen n factor, it is possible to find the ink surface coverages that minimize a difference metric such as the sum of square differences between a given measured reflection spectrum and the reflection spectrum predicted by the YNSN model. Such fitted ink surface coverages are referred to as *effective ink surface coverages* and are usually larger than the intended *nominal ink surface coverages*. They yield a physical dot gain which is defined as the difference between the effective and corresponding nominal ink surface coverages.

Physical dot gain depends on the printing process, the inks, the paper, and also on the ink superposition condition, i.e. the specific superposition of an ink halftone and solid inks. Most previous approaches rely on 1-D mappings which describe the effective surface coverage of a given ink as a non-linear function of the nominal coverage of this ink only. The resulting 1D mappings form the tone reproduction curves [1][10].

The YNSN model has been used by many researchers for the characterization of printing systems [7]-[16]. It therefore plays a significant role in building color management systems.

III. THE INK SPREADING MODEL

In contrast to most ink spreading models proposed in the literature, we use an ink spreading model that takes all possible ink superposition conditions into consideration. The amount of dot gain of an ink depends on whether the ink halftone is printed alone on paper or in superposition with one or more other inks [4][17].

The proposed ink spreading model relies on ink spreading curves. An ink spreading curve maps the nominal surface coverages of ink halftones into their effective surface coverages, i.e. to the surfaces that the ink halftones effectively

cover after being printed. There is one ink spreading curve for each ink halftone in each superposition condition. For example, a cyan halftone may be printed alone, c ; superposed with solid magenta, c/m ; with solid yellow, c/y ; with solid black, c/k ; with solid magenta and solid yellow, c/my ; with solid magenta and solid black, c/mk ; with solid yellow and solid black, c/yk ; and with solid magenta, yellow and black, c/myk . There are 8 different ink spreading curves for each ink, yielding a total of 32 ink spreading curves. However, since any halftone superposed with solid black yields a reflection spectrum very close to the reflection spectrum of solid black, ink spreading curves where one ink halftone is superposed with solid black are discarded [5]. Table I lists all the considered ink spreading curves.

Table I. List of the considered ink spreading curve indicia.

Cyan	Magenta	Yellow	Black	
c	m	y	k	k/y
c/m	m/c	y/c	k/c	k/cy
c/y	m/y	y/m	k/m	k/my
c/my	m/cy	y/cm	k/cm	k/cmy

In previous works of the present authors [4][5][17][18], each ink spreading curve is calibrated using one or more so-called calibration patches, e.g. a halftone at 50% nominal surface coverage. Each halftone calibration patch determines the effective surface coverage obtained when asking the printer to print the halftone at its nominal surface coverage. It determines one point of the ink spreading curve. Such effective surface coverages are fitted by minimizing a difference metric such as the sum of square differences between the measured and predicted spectral reflectance components of the corresponding calibration patches. The ink spreading curves are then linearly interpolated between the calibrated effective surface coverages. In order to avoid the ambiguity between chromatic black and pure black [18], the spectral measurements span both the visible wavelength range (380-730 nm) and the near infrared (NIR) wavelength range (730-850 nm). The NIR wavelength range enables distinguishing the light absorbing pigment-based black ink from the superposition of CMY inks, which are dye-based and do not absorb light in the NIR wavelength range.

In the present contribution, rather than using linear interpolation, we use the following analytical description for the ink spreading curves:

$$\begin{aligned} f_{i/jk}(u_i, v_{i/jk}) &= u_i + (4v_{i/jk} - 2)(1 - u_i)u_i \\ &= u_i^2(2 - 4v_{i/jk}) + u_i(4v_{i/jk} - 1) \end{aligned} \quad (3)$$

where u_i is the nominal surface coverage of ink i , $f_{i/jk}$ is the ink spreading curve of ink i superposed with solid inks j and k , and $v_{i/jk}$ is the effective surface coverage at 50% nominal surface coverage, also called mid-point of the ink spreading curve. Equation (3) represents a parabola that passes through the three points: (0,0), (0.5, $v_{i/jk}$), and (1,1). An ink spreading curve is therefore completely specified by the halftone at 50% nominal surface coverage. Moreover, it is a monotonically increasing function if $v_{i/jk} \in [0.25, 0.75]$.

In order to obtain the effective surface coverages of the ink dots forming a color halftone, we weight the contributions of the different ink spreading curves as follows. The effective coverage of ink dot i superposed with solid inks j and k is the weighted average of the ink spreading functions f_i , f_{ij} , f_{ik} , and f_{ijk} . The weights are computed according to the surface coverages of the underlying colorants formed by inks j and k . In (4) for example, $(1-m')(1-y')$, $m'(1-y')$, $(1-m')y'$, and $m'y'$ express, respectively, the surface coverage of colorants white, magenta, yellow, and red superposed with the cyan halftone layer. Since a cyan, magenta, or yellow halftone over solid black is assumed to yield black, the superposition conditions corresponding to an ink halftone over solid black have been discarded. We have therefore 4 superposition conditions for the cyan, magenta and yellow ink halftones and 8 superposition conditions for the black ink halftone.

We solve (4) iteratively, starting by assigning the nominal ink halftone coverages (c, m, y, k) to the effective ink halftone coverages (c', m', y', k') [5]. Four to five iterations ensure sufficient convergence to determine the effective ink halftone surface coverages.

$$\begin{aligned} c' &= (1-m')(1-y') f_c(c) \\ &+ m'(1-y') f_{c/m}(c) \\ &+ (1-m')y' f_{c/y}(c) \\ &+ m'y' f_{c/my}(c) \\ m' &= (1-c')(1-y') f_m(m) \\ &+ c'(1-y') f_{m/c}(m) \\ &+ (1-c')y' f_{m/y}(m) \\ &+ c'y' f_{m/cy}(m) \\ y' &= (1-c')(1-m') f_y(y) \\ &+ c'(1-m') f_{y/c}(y) \\ &+ (1-c')m' f_{y/m}(y) \\ &+ c'm' f_{y/cm}(y) \\ k' &= (1-c')(1-m')(1-y') f_k(k) \\ &+ c'(1-m')(1-y') f_{k/c}(k) \\ &+ (1-c')m'(1-y') f_{k/m}(k) \\ &+ c'm'(1-y') f_{k/cm}(k) \\ &+ (1-c')(1-m')y' f_{k/y}(k) \\ &+ c'(1-m')y' f_{k/cy}(k) \\ &+ (1-c')m'y' f_{k/my}(k) \\ &+ c'm'y' f_{k/cmy}(k) \end{aligned} \quad (4)$$

IV. THE INK SPREADING ENHANCED YULE-NIELSEN MODIFIED SPECTRAL NEUGEBAUER MODEL (IS-YNSN)

The spectral reflection prediction model used in the present contribution is the Yule-Nielsen modified Spectral Neugebauer model enhanced with the ink spreading model (IS-YNSN) presented in Section III [4].

Spectral predictions using the IS-YNSN model are performed according to Fig. 2. For given nominal ink surface coverages c, m, y, k , we obtain effective surface coverages c', m', y', k' by weighting the ink spreading curves $f_i(c)$ to $f_{k/cmy}(k)$ according to the surface coverages of the colorants contributing to that color halftone [Equations (4)]. With the

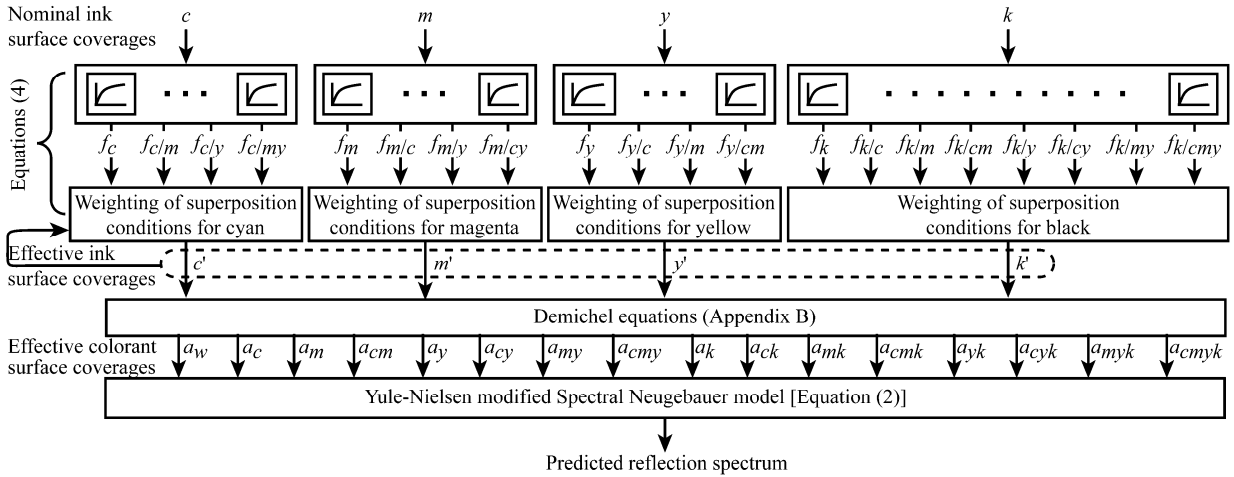


Fig. 2. The ink spreading enhanced Yule-Nielsen modified Spectral Neugebauer model with nominal ink surface coverages c , m , y , and k ; ink spreading curves f_{ijk} of ink i superposed with solid inks j and k ; effective ink surface coverages c' , m' , y' , and k' ; and effective colorant surface coverages a_w to a_{cmk} .

Demichel equations (Appendix B), we then compute the corresponding effective surface coverages of the colorants forming that color halftone. With these effective colorant coverages, the YNSN model calculates the predicted reflection spectrum.

V. CALIBRATION OF THE INK SPREADING MODEL USING REFLECTION SPECTRA ACQUIRED WITHIN PRINTED COLOR IMAGES

The goal of the present contribution is to calibrate the ink spreading curves used by the IS-YNSN spectral prediction model, i.e. to set the mid-points of the 20 ink spreading curves for CMYK prints using a set of reflection spectra acquired from tiles located within printed color images, further referred to as *image tiles*, instead of the reflection spectra of specific uniform calibration patches. The set of image tiles used for calibration is further referred to as the *image calibration set*, or *image calibration tiles*. The reflection spectra of specially conceived uniform calibration patches composed of one ink halftone superposed with paper or superposed with other solid inks is further referred to as the *classical calibration set*, or *classical calibration patches*. The reflection spectra of the solid colorants (Neugebauer primaries) and the Yule-Nielsen n factor are assumed to be known for the target printing process.

The problem with image tiles is that not all superpositions of inks and halftones are necessarily present. For example, if an image does not contain any cyan, it is not possible to calibrate the ink spreading curves of the cyan ink. When the contribution of an ink to a given image calibration tile is weak, the minimization algorithm tends to induce large variations of the values of the corresponding ink spreading curves in order to influence the difference metric. The consequence is that the ink spreading curves are set to artificially large values that do not reflect the actual dot gain. Such calibrations may be able to accurately predict image tiles similar to the calibration set, but fail to correctly predict image tiles of other colors [19].

To avoid this problem, we introduce weights, one for each ink spreading curve. A weight evaluates whether its ink spreading curve is relevant for predicting the image tiles of the calibration set or not. If modifying a given ink spreading curve changes significantly some of the predicted reflection spectra, its associated weight should be close to 1. If on the contrary the predicted spectra do not significantly change, the weight should be close to 0. The weights are used to define upper and lower bounds for the mid-points of the ink spreading curves. As seen in Section III, the mid-points must be in the interval $[0.25 \ 0.75]$ in order to obtain monotonically increasing ink spreading curves. We modify the definition of the bounds for a given ink spreading curve as follows:

$$0.5 - 0.25 \cdot w_{i/jk} \leq v_{i/jk} \leq 0.5 + 0.25 \cdot w_{i/jk} \quad (5)$$

where $w_{i/jk}$ represents the weight of ink halftone i superposed with solid inks j and k . When the weight is equal to 1, the interval for the mid-point is not reduced. When the weight is equal to 0, i.e. when modifying the ink spreading curve does not modify the predicted spectra, the interval is reduced to a single mid-point, i.e. 0.5. When an ink spreading curve contributes only slightly to the calibration set, its weight is low and the interval for its mid-point is reduced. This prevents the fitting procedure from inducing large mid-point variations when minimizing the metric expressing the distance between predicted and measured reflection spectra.

Given a tile p of the image calibration set, let $u_{i,p}$ be the nominal coverage and $u_{i,p}'(v_i, v_{ij}, v_{ik}, v_{ijk})$ be the effective coverage of ink i within tile p . The weight associated to ink spreading curve f_{ijk} of halftone ink i superposed with solid inks j and k is defined as the following gradient:

$$w_{i/jk,p} = \frac{\partial u_{i,p}'}{\partial v_{i/jk}} \quad (6)$$

Since ink spreading curve f_{ijk} is fully determined by its mid-point v_{ijk} , the gradient in (6) expresses the influence of ink spreading curve f_{ijk} on the resulting effective surface coverage $u_{i,p}'$ of ink i within tile p .

Since a calibration set is composed of several tiles, we define the weight associated to ink spreading curve $f_{i/jk}$ for the full image calibration set as the maximum of the weights of all the tiles:

$$w_{i/jk} = \max_p [w_{i/jk,p}] = \max_p \frac{\partial u_{i,p}}{\partial v_{i/jk}} \quad (7)$$

We take the maximum of the derivatives among all the tiles because the tiles with a high weight have the largest influence on the metric minimized by the ink spreading curve mid-point fitting algorithm, i.e. when there is at least one high weight tile and low weight tiles, the ink spreading curve mid-point is mainly fitted by the high weight tile.

Let us show that the weights defined according to (7) are comprised between 0 and 1. We calculate the derivative of an ink spreading curve with respect to its mid-point using (3):

$$\frac{\partial f_{i/jk}}{\partial v_{i/jk}} = \frac{\partial}{\partial v_{i/jk}} [u_i + (4v_{i/jk} - 2)(1 - u_i)u_i] = 4(1 - u_i)u_i \quad (8)$$

Equation (8) depends neither on the superposition condition nor on the mid-point value, but only on the nominal surface coverage of the considered ink. Since u_i is a nominal surface coverage comprised between 0 and 1, the derivative reaches a maximum of 1 when $u_i = 0.5$ and a minimum of 0 when $u_i = 0$ or $u_i = 1$.

Let us now calculate the derivative of the effective surface coverages with respect to the mid-point of a given ink spreading curve. This derivative is 0 for all effective coverages except for the effective coverage affected by the chosen ink spreading curve. Let us for example consider the cyan ink. The effective coverage of cyan c' is influenced by four ink spreading curves: f_c , $f_{c/m}$, $f_{c/y}$, and $f_{c/my}$. With (4) and (8), the derivatives of the cyan effective coverage with respect to v_c , $v_{c/m}$, $v_{c/y}$, and $v_{c/my}$ are:

$$\frac{\partial c'}{\partial v_c} = (1 - m')(1 - y') \frac{\partial f_c(c)}{\partial v_c} = (1 - m')(1 - y') \cdot 4c(1 - c) \quad (9)$$

$$\frac{\partial c'}{\partial v_{c/m}} = m'(1 - y') \frac{\partial f_{c/m}(c)}{\partial v_{c/m}} = m'(1 - y') \cdot 4c(1 - c) \quad (10)$$

$$\frac{\partial c'}{\partial v_{c/y}} = (1 - m')y' \frac{\partial f_{c/y}(c)}{\partial v_{c/y}} = (1 - m')y' \cdot 4c(1 - c) \quad (11)$$

$$\frac{\partial c'}{\partial v_{c/my}} = m'y' \frac{\partial f_{c/my}(c)}{\partial v_{c/my}} = m'y' \cdot 4c(1 - c) \quad (12)$$

These derivatives represent the weights w_c , $w_{c/m}$, $w_{c/y}$, and $w_{c/my}$ for tile p given by its nominal surface coverages c , m , y , k . The nominal coverages are known from prepress image data and the effective coverages are obtained with the YNSN model, i.e. the effective coverages are found by minimizing the sum of square differences between the measured reflection spectra components of the considered image tile and the ones predicted by the YNSN model [18]. Eqs. (9)-(12) are therefore fully determined. Moreover, all the variables are either nominal or effective surface coverages which are comprised

between 0 and 1. As shown above, $4c(1-c)$ is also comprised between 0 and 1. Equations (9)-(12) are therefore also comprised between 0 and 1. This demonstrates that the weights defined in (7) are indeed comprised between 0 and 1.

It is also interesting to observe the nominal surface coverages when a weight reaches its maximum, i.e. when it is equal to 1. If we consider the weight $\partial c'/\partial v_c$ associated with the ink spreading curve $f_c(c)$ of cyan halftones printed on paper, expressed by (9), it reaches its maximum when $m' = y' = 0$ and when $c = 0.5$. As $m' = 0$ implies $m = 0$, a patch maximizes the weight of the cyan $f_c(c)$ ink spreading curve only when its nominal surface coverages are $c = 0.5$, $m = 0$ and $y = 0$. These correspond to the nominal surface coverages of the patch used to calibrate the cyan ink spreading curve in the classical calibration set. In the case of cyan superposed with solid magenta, computed by (10), the maximal weight is obtained with $c = 0.5$, $m = 1$ and $y = 0$. Similar statements are valid for the other two superposition conditions. Therefore, the classical calibration set maximizes the weights of all the ink spreading curves. Hence, when using the classical calibration set, the calibration of the ink spreading model is not constrained, i.e. the weights are always 1.

Let us now present the complete calibration procedure. We propose a least-squares approach to calibrate the ink spreading curves given the reflection spectra of an image calibration set. First, the effective surface coverages (c' , m' , y' , k') of each image calibration tile are fitted by using the YNSN model (see paragraph following (12)). Then, the weights associated to the ink spreading curves are computed using (7), with examples of the weights of a single tile given in (9) to (12). Each weight $w_{i/jk}$ defines the bounds for its associated ink spreading curve mid-point $v_{i/jk}$. Finally, the mid-points of the ink spreading curves are determined using a constrained least-squares procedure where the constraints are the bounds of the different mid-points. The constrained least-squares equations are derived from (4). There is one least-squares equation per effective ink surface coverage. For example, let us take the equation computing the cyan effective surface coverage. Substituting (3) in (4) yields:

$$\begin{aligned} c' &= (1 - m') (1 - y') (c + (4v_c - 2)(1 - c)c) \\ &+ m' (1 - y') (c + (4v_{c/m} - 2)(1 - c)c) \\ &+ (1 - m') y' (c + (4v_{c/y} - 2)(1 - c)c) \\ &+ m' y' (c + (4v_{c/my} - 2)(1 - c)c) \end{aligned} \quad (13)$$

$$\text{Let } \xi = [(1 - m')(1 - y') \quad m'(1 - y') \quad (1 - m')y' \quad m'y'].$$

Equation (13) is rewritten in matrix form:

$$c' + \xi \begin{bmatrix} 2(1 - c)c - c \\ 2(1 - c)c - c \\ 2(1 - c)c - c \\ 2(1 - c)c - c \end{bmatrix} = 4(1 - c)c \xi \begin{bmatrix} v_c \\ v_{c/m} \\ v_{c/y} \\ v_{c/my} \end{bmatrix} \quad (14)$$

Since the sum of all terms of ξ is one, (14) becomes:

$$c' + 2(1 - c)c - c = 4(1 - c)c \xi [v_c \quad v_{c/m} \quad v_{c/y} \quad v_{c/my}]^T \quad (15)$$

Equation (15) has the form $b_p = A_p x$ where A_p is the row

vector $4(1-c)c\xi$ and x the vector with the unknown ink spreading mid-point values. Knowing both nominal and effective surface coverages, each tile of the calibration set forms one line of matrix A and one element of vector b . Considering all the calibration tiles, we obtain the following constrained least-squares problem:

$$x_{\min} = \arg \min_x (\|b - Ax\|) \text{ such that } \begin{cases} v_{i/jk} \leq 0.5 + 0.25 \cdot w_{i/jk} \\ v_{i/jk} \geq 0.5 - 0.25 \cdot w_{i/jk} \end{cases} \quad (16)$$

where x_{\min} is the vector containing the calibrated mid-points of the ink spreading curves. Such problems are readily solved using existing algorithms [20][21], possibly implemented by computer programs such as Matlab. Note that it is also possible to perform the above calibration procedure using a calibration set composed of a mixture of classical calibration patches and image tiles, or even composed of classical calibration patches only.

VI. SELECTION OF IMAGE CALIBRATION AND TEST TILES

Before verifying the accuracy of the proposed calibration on image tiles, we need to select tiles as uniform as possible from the available images, well distributed across the color space. For each image, we form two sets of tiles. The first set contains calibration tiles and the second set test tiles.

The first step consists in scanning each image horizontally and vertically in 2 mm steps. Successive 5 mm large square tiles form the candidate tiles from which calibration and test tiles are selected. Each tile is associated a uniformity value. We define the uniformity of a given color area as the RMS of the standard deviation of the CIELAB pixel values located within the considered image tile:

$$s = \sqrt{(\sigma(L^*)^2 + \sigma(a^*)^2 + \sigma(b^*)^2) / 3} \quad (17)$$

The calibration set associated with a given image contains approximately 50 of the most uniform tiles, i.e. those with the smallest s value, with the additional condition that each tile has no other tile within $\Delta E_{ab} < 2$ and no more than one other tile within $\Delta E_{ab} < 6$. The test set associated with that image contains the most uniform 30 tiles that are not part of the calibration set, and with the additional condition that each tile has no other tile within $\Delta E_{ab} < 6$.

We use the same images and the same image tile selections presented in our previous contribution [19], where the ink spreading curves were fitted without considering their relevance for a given image calibration set, i.e. without introducing constraints on the ink spreading curve mid-points.

VII. SETUP OF THE EXPERIMENTS

The experiments are performed on a Canon Pixma Pro 9500 printer, with color images printed on Canon MP-101 matte paper with classical clustered dot halftoning, at a resolution of 600 dpi and a screen frequency of 100 lpi. The black ink is pigment based and absorbs in the near infrared wavelength range (cartridge PGI-9MBK). Reflectance spectra are measured with a Datacolor MF-45 spectrophotometer

(geometry: 45°d:0°, i.e. 45° directed incident light and capture at 0°) at 10 nm intervals between 380 nm and 850 nm.

The reflectances of the printed colorants (Neugebauer primaries) have been measured. The Yule-Nielsen n factor is set to a suitable value according to the classical calibration, 7.8 in the current case. Note that both the reflectances of the colorants and the Yule-Nielsen n factor can be tabulated for each combination of inks and paper.

The “fruits” and “textile” images are printed using 3 inks only (CMY) and using 4 inks (CMYK). In each case, 4 different sets of tiles are measured: the calibration and test sets of the “fruits” image, and the calibration and test sets of the “textile” image.

VIII. CALIBRATION OF THE INK SPREADING CURVES WITH SPECTRA MEASURED ON THE SELECTED IMAGE TILES

The algorithm presented in Section V aims at calibrating the ink spreading model, i.e. at setting the ink spreading curves as accurately as possible, without printing specially conceived halftone patches. According to Equation (4), there are 12 ink spreading curves to fit for the CMY prints, and 20 ink spreading curves for the CMYK prints. To each ink spreading curve $f_{i/jk}$ mapping nominal to effective surface coverages in a given superposition condition we associate a dot gain curve $g_{i/jk}$ with the dot gain being defined as the effective surface coverage minus the nominal surface coverage:

$$g_{i/jk}(u_i) = f_{i/jk}(u_i, v_{i/jk}) - u_i = (4v_{i/jk} - 2)(1 - u_i)u_i \quad (18)$$

In the same way, the bounds associated with dot gain curve $g_{i/jk}$ are defined as follows based on (5) and (18):

$$0.25 \cdot w_{i/jk} \leq g_{i/jk}(0.5) = v_{i/jk} - 0.5 \leq 0.25 \cdot w_{i/jk} \quad (19)$$

In both CMY and CMYK cases, we consider five different calibrations. The first case, where all the ink spreading curves are arbitrarily set to 10% dot gain, is referred to as the *no calibration* case. The second calibration is called the *minimal classical calibration* and is calibrated using a single uniform patch per ink spreading curve. This single patch yields the effective surface coverage at 50% nominal surface coverage and is referred to as the *50% patch*. For example, the 50% patch of the f_{cm} ink spreading curve is 50% cyan superposed with solid magenta. Therefore, the minimal classical calibration requires 12 calibration patches for CMY prints, and 20 calibration patches for CMYK prints. The third calibration, referred to as the *extended classical calibration*, includes the 25%, 50% and 75% uniform patches for the calibration of each ink spreading curve. Such a calibration requires 36 patches for CMY prints and 60 patches for CMYK prints. The fourth and fifth calibrations use the “fruits” image calibration set and the “textile” image calibration set, respectively. These last two calibrations are also referred to as the *image calibrations*.

Fig. 3 compares no calibration, minimal classical calibration and extended classical calibration. The cyan and magenta dot gain curves are similar for the minimal and extended classical calibrations. However, the yellow and

black dot gain curves show significant variations. This indicates that the 50% patches are enough to characterize the cyan and magenta dot gain curves, but not the yellow and black dot gain curves.

Fig. 4 compares the extended classical, the fruits and the textile calibrations in the CMYK case. The figure shows that half the dot gain curves of both image calibrations agree well with the extended classical calibration. There are also a few cases where the dot gain curves of the image calibrations reach their respective bounds computed using (19), especially the black ink spreading curves. However, this occurs only when the bounds are tight. When the bounds are loose, the fitted ink spreading curves are located close to the extended classical calibration and away from the bounds. This is the expected behavior and confirms that the bounds of a given ink spreading curve are loose only when the calibration set contains at least one tile highly relevant for that ink spreading curve.

The effect of the constraints can be seen in Fig. 5. When the constraints are not used, five black and one yellow dot gain curves are set outside the defined bounds, with three of them even reaching the original bound of $\pm 25\%$. These dot gain curves are also the ones with the strictest bounds, meaning that the calibration set does not contain tiles that are relevant enough to calibrate these dot gain curves. The unconstrained calibration procedure sets the ink spreading curves to extreme values in order to have a small gain of accuracy. This gain improves only the accuracy of the image calibration set. When predicting another set of tiles, all gains are lost and the predictions are poor.

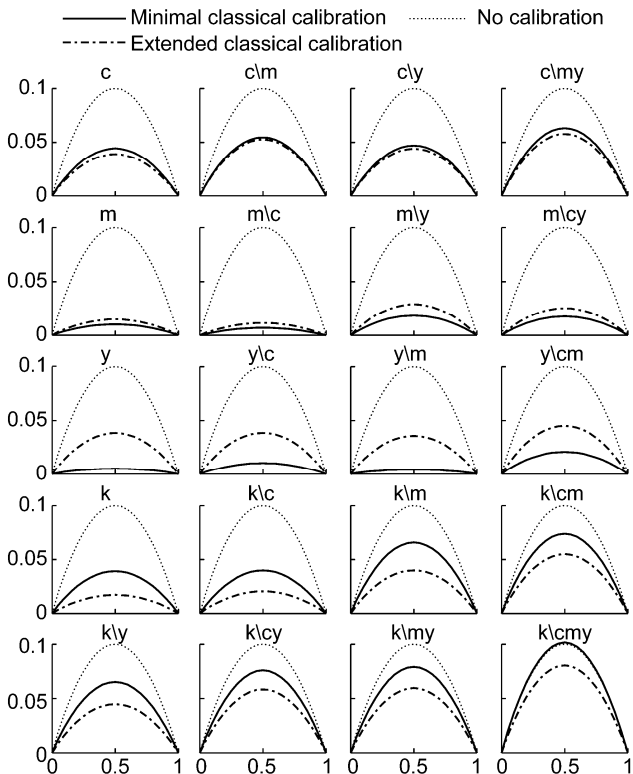


Fig. 3. CMYK dot gain curves of the minimal classical calibration, extended classical calibration and no calibration

IX. PREDICTION ACCURACY

The calibrations performed in Section VIII are tested by comparing the difference between predicted and measured reflectances for different test sets. In the CMY case, we predict the CMY test sets of the “fruits” and “textile” images and a set composed of 125 CMY uniform patches whose nominal surface coverages are all the CMY combinations at 0%, 25%, 50%, 75%, or 100%. In the CMYK case, we predict the CMYK test sets of the “fruits” and “textile” images, a set composed of 625 CMYK patches whose nominal surface coverages are all the CMYK combinations at 0%, 25%, 50%, 75%, or 100%, and a fourth set, further referred to as the 125 UCR set, composed of 125 CMYK patches corresponding to the 125 CMY set, but with nominal surface coverages obtained by converting the original CMY coverages to CMYK using a standard under color removal algorithm.

The reflection spectrum of each image tile or uniform patch of the selected sets is predicted and then compared to the corresponding measured reflection spectrum using the ΔE_{94} metric [22]. For each measurement set, we compute the following statistics: average, 95 percentile and maximum ΔE_{94} between measured and predicted spectra. The results are shown in the tables located in Appendix A. Table II shows the results for the CMY tests and Table III shows the results for the CMYK tests. In Figs. 6a-6c, the prediction accuracy is defined as the inverse of the average ΔE_{94} .

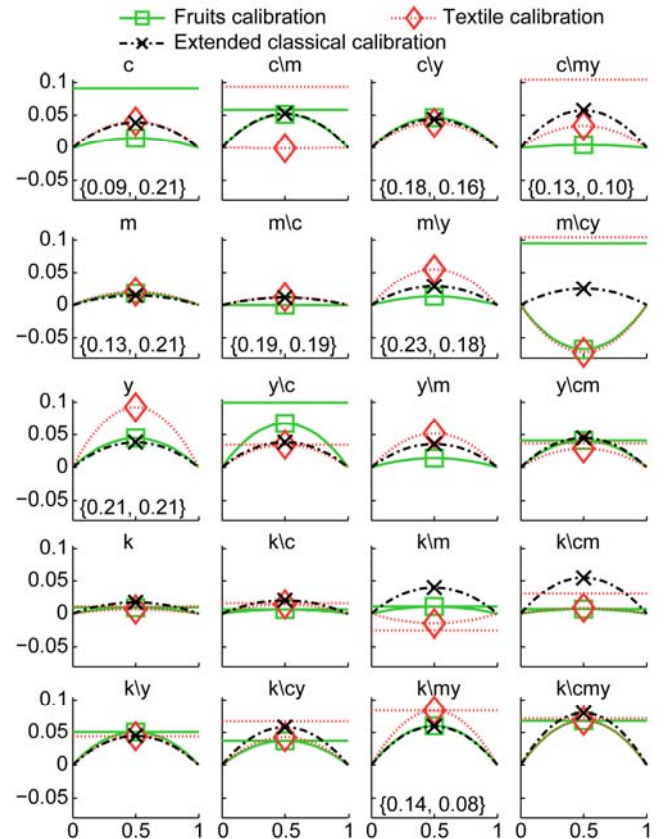


Fig. 4. CMYK dot gain curves of the fruits, textile and extended classical calibrations. The upper bounds of the fruits (F_B) and textile (T_B) dot gain curves are indicated as horizontal lines or with the values $\{F_B, T_B\}$ respectively.

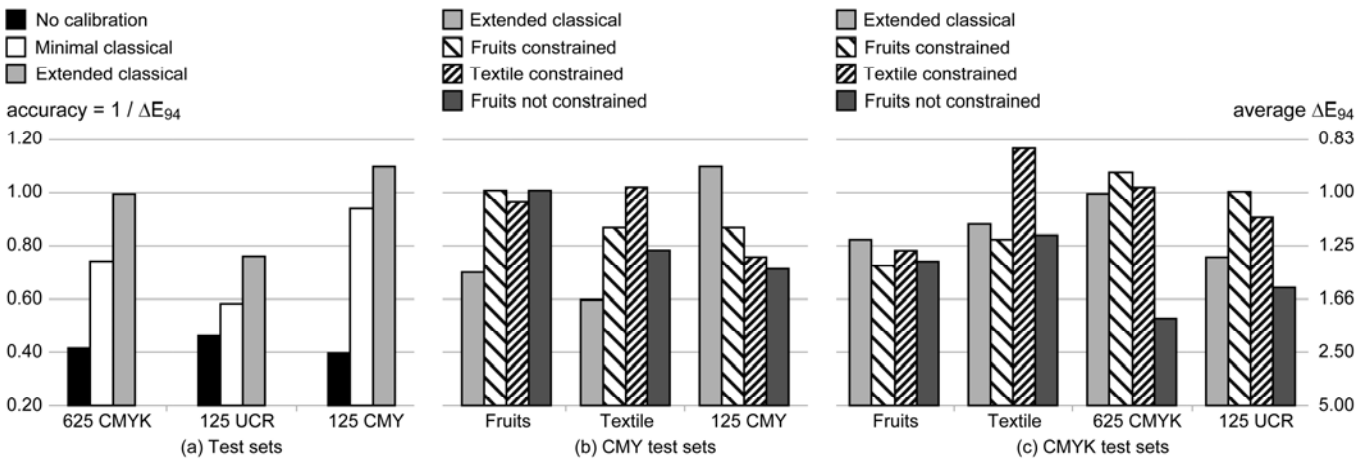


Fig. 6. Comparison of the accuracy of (a) “no calibration”, minimal classical calibration and extended classical calibration on the 625 CMYK, 125 UCR and 125 CMY test sets (b) extended classical, constrained textile, constrained fruits, and unconstrained fruits calibrations on the CMY fruits and textile test tiles and on the 125 CMY test set (c) extended classical, constrained textile, constrained fruits, and unconstrained fruits calibrations on the CMYK fruits and textile test tiles, and on the 625 CMYK and 125 UCR test sets.

Fig. 6a shows the accuracy of “no calibration”, minimal classical calibration and extended classical calibration for one CMY and two CMYK test sets. As expected the “no calibration” case yields the worst results and the extended classical calibration yields significantly better results than the minimal classical calibration, especially for the CMYK test sets, outlining the fact that, for the considered PixmaPro 9500 ink jet printer, the 25% and 75% surface coverage patches are important for classical calibrations.

Figs. 6b-6c show the accuracy difference between the extended classical, fruits, and textile calibrations, as well as the fruits calibrations without constraints. These calibrations are compared on the CMY fruits, CMY textile, and 125 CMY test sets in Fig. 6b and on the CMYK fruits, CMYK textile, 625 CMYK, and 125 UCR test sets in Fig. 6c. In Fig. 6b, the results are as expected: The fruits calibrations have the best accuracy on the fruits test set, the textile calibration on the textile test set, and the extended classical calibration on the 125 CMY test. Moreover, the constrained fruits calibration has a significantly higher prediction accuracy on the 125 CMY test set than the unconstrained fruits calibration.

In Fig. 6c, the extended classical and images calibrations, both with and without constraints, accurately predict both the CMYK textile and fruits test sets. The textile calibration is particularly accurate on the textile test set. The fact that the fruits calibration does not display such an accuracy on the fruits test set is due to the fact that the fruits test set is more different from the fruits calibration set (average distance between each test tile and its nearest calibration tile is $\Delta E_{94} = 2.94$) than the textile test set from the textile calibration set (average distance $\Delta E_{94} = 1.60$). The constraints are extremely important when predicting both the 625 CMYK set and the 125 UCR set. Removing the constraints leads to a sharp drop of accuracy. This indicates that the constraints considerably improve the accuracy of a calibration when predicting the reflection spectra of a set of patches or tiles significantly different from the calibration tiles.

Surprisingly, the image calibrations with constraints have predictions as accurate as the extended classical calibration or even better predictions in the case of the 625 CMYK or 125 UCR test sets. This indicates that calibrating the ink spreading model based on reflection spectra of image halftones is a valid approach. Whereas the classical calibration uses artificially crafted patches—there are at the macroscopic level few to no occurrences of superpositions of one halftone and solid inks in a conventional image—relying on tiles directly taken from

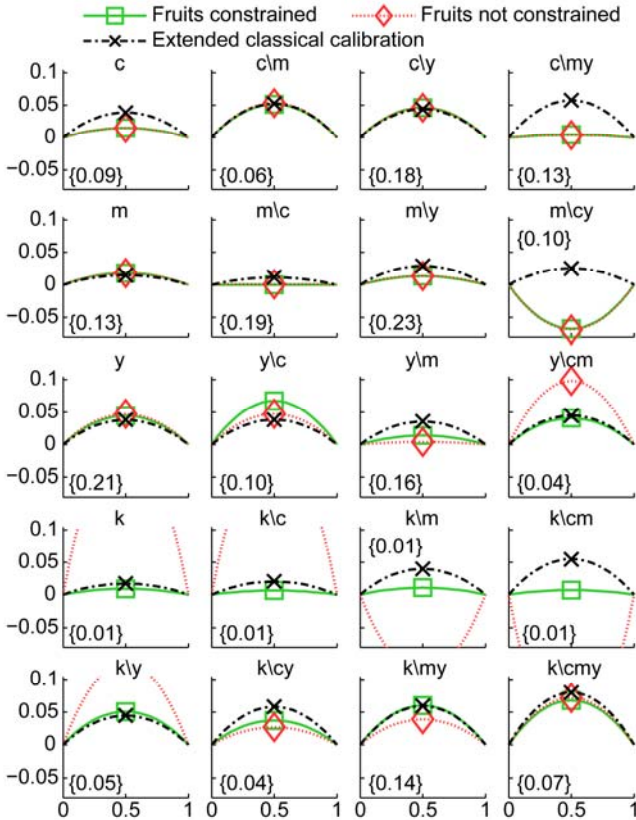


Fig. 5. CMYK dot gain curves of the constrained fruits calibration, unconstrained fruits calibration, and extended classical calibration. The bounds of the constrained fruits calibration are given as $\{F_B\}$.

real images can achieve higher accuracy because these image tiles better represent the normal operational conditions of the reproduction device.

X. CONCLUSION

When correctly calibrated, today's spectral reflection prediction models are able to accurately predict the reflection spectra of printed color image tiles. However, the required calibration procedures remain difficult and cumbersome because they require printing specially conceived uniform calibration patches which use space and need to be removed from the final product.

The present contribution aims at calibrating the ink spreading model using spectral data acquired within printed images. Image tiles as uniform as possible are selected within printed images and the ink spreading model is calibrated with the measurements of the selected calibration image tiles.

Depending on the available calibration image tiles, certain ink spreading curves cannot be reliably calibrated because these ink spreading curves are not relevant in the prediction of the calibration tiles. We therefore establish a simple relevance metric which relies on the nominal surface coverages of the considered halftone and on the effective surface coverages of the superposed other inks. Relying on this metric, we create bounds for the mid-points of the fitted ink spreading curves. When the relevance is low, the effective surface coverages remain close to the nominal surface coverages. This metric reaches its maximum relevance at 50% halftone surface coverage on top of solid inks, which corresponds to the classical calibration patches. Therefore, the classical calibration is a subset of the proposed constrained image tile calibration approach.

The performed experiments demonstrate that the new constraint-based calibration procedure is reliable when predicting patches significantly different from the calibration patches. Moreover, the predictions of patches similar to the calibration patches remain as accurate with the added constraints as without. Finally, the image calibration can be more accurate than a classical calibration when predicting test sets composed of uniform patches distributed over the entire printing gamut of the reproduction device, suggesting that the classical calibration patches, despite incorporating the highest relevant patches formed by halftones superposed with solid inks, are not necessarily the most adequate patches to calibrate the ink spreading model.

Some redundancy remains between the Yule-Nielsen n factor and the ink spreading model. Characterizing how the ink spreading curves are modified when the n factor is modified may lead to the definition of additional constraints enabling one to further reduce the degrees of freedom of the ink spreading model and to simplify the calibration procedure. Further topics of interest comprise the selection of optimal calibration tiles from a given set of candidate color image tiles and the use of non-uniform image tiles for the calibration procedure.

APPENDIX A

Table II. Prediction accuracy for different CMY test sets. The statistics show the average, 95 percentile and maximum ΔE_{94} .

CMY test sets Calibrations	ΔE_{94}		
	avg	95%	max
CMY test set fruits			
<i>No calibration</i>	3.16	4.49	4.92
<i>Minimal calibration</i>	1.57	2.72	2.98
<i>Extended calibration</i>	1.32	2.51	2.81
<i>Fruits with constraints</i>	1.02	1.84	1.88
<i>Textile with constraints</i>	1.12	2.40	2.62
<i>Fruits no constraints</i>	1.02	1.74	1.87
<i>Textile no constraints</i>	1.14	2.61	2.95
CMY test set textile			
<i>No calibration</i>	3.34	5.11	5.29
<i>Minimal calibration</i>	1.98	3.41	3.49
<i>Extended calibration</i>	1.68	2.94	3.28
<i>Fruits with constraints</i>	1.15	2.01	2.02
<i>Textile with constraints</i>	0.98	1.82	2.24
<i>Fruits no constraints</i>	1.28	3.26	3.40
<i>Textile no constraints</i>	0.90	1.75	1.90
125 CMY test set			
<i>No calibration</i>	2.51	4.31	4.48
<i>Minimal calibration</i>	1.07	2.79	3.43
<i>Extended calibration</i>	0.91	1.81	2.36
<i>Fruits with constraints</i>	1.16	2.76	3.95
<i>Textile with constraints</i>	1.33	3.18	4.23
<i>Fruits no constraints</i>	1.41	3.85	4.51
<i>Textile no constraints</i>	1.71	4.42	5.62

Table III. Prediction accuracy for different CMYK test sets. The statistics show the average, 95 percentile and maximum ΔE_{94} .

CMYK test sets Calibrations	ΔE_{94}		
	avg	95%	max
CMYK test set fruits			
<i>No calibration</i>	1.66	3.53	4.12
<i>Minimal calibration</i>	1.61	2.85	3.26
<i>Extended calibration</i>	1.22	2.40	3.34
<i>Fruits with constraints</i>	1.38	2.55	4.67
<i>Textile with constraints</i>	1.27	2.62	4.26
<i>Fruits no constraints</i>	1.35	2.54	4.59
<i>Textile no constraints</i>	1.32	2.93	4.18
CMYK test set textile			
<i>No calibration</i>	1.56	3.31	3.37
<i>Minimal calibration</i>	1.50	2.50	2.95
<i>Extended calibration</i>	1.14	1.72	2.55
<i>Fruits with constraints</i>	1.21	2.11	2.17
<i>Textile with constraints</i>	0.86	1.38	1.57
<i>Fruits no constraints</i>	1.19	2.07	2.24
<i>Textile no constraints</i>	0.81	1.46	1.49
625 CMYK test set			
<i>No calibration</i>	2.41	3.48	3.94
<i>Minimal calibration</i>	1.35	2.50	3.21
<i>Extended calibration</i>	1.01	1.87	2.43
<i>Fruits with constraints</i>	0.93	1.99	3.62
<i>Textile with constraints</i>	0.98	2.23	3.56
<i>Fruits no constraints</i>	1.91	6.07	10.37
<i>Textile no constraints</i>	1.99	5.69	8.34
125 UCR test set			
<i>No calibration</i>	2.16	3.63	4.20
<i>Minimal calibration</i>	1.73	3.17	3.69
<i>Extended calibration</i>	1.31	2.30	2.79
<i>Fruits with constraints</i>	0.99	1.83	2.56
<i>Textile with constraints</i>	1.10	2.11	2.40
<i>Fruits no constraints</i>	1.56	4.06	6.03
<i>Textile no constraints</i>	2.03	5.24	6.99

APPENDIX B

Demichel equations for 4 inks, where c , m , y , and k are the ink surface coverages of the cyan, magenta, yellow, and black inks, respectively; and a_w , a_i , a_{ij} , and a_{ijk} are the fractional area covered by paper, single ink i , the superposition of inks i and j , and the superposition of inks i , j and k , respectively.

$$\begin{aligned}
 a_w &= (1-c) \cdot (1-m) \cdot (1-y) \cdot (1-k) \\
 a_c &= c \cdot (1-m) \cdot (1-y) \cdot (1-k) \\
 a_m &= (1-c) \cdot m \cdot (1-y) \cdot (1-k) \\
 a_{cm} &= c \cdot m \cdot (1-y) \cdot (1-k) \\
 a_y &= (1-c) \cdot (1-m) \cdot y \cdot (1-k) \\
 a_{cy} &= c \cdot (1-m) \cdot y \cdot (1-k) \\
 a_{my} &= (1-c) \cdot m \cdot y \cdot (1-k) \\
 a_{cmy} &= c \cdot m \cdot y \cdot (1-k) \\
 a_k &= (1-c) \cdot (1-m) \cdot (1-y) \cdot k \\
 a_{ck} &= c \cdot (1-m) \cdot (1-y) \cdot k \\
 a_{mk} &= (1-c) \cdot m \cdot (1-y) \cdot k \\
 a_{cmk} &= c \cdot m \cdot (1-y) \cdot k \\
 a_{yk} &= (1-c) \cdot (1-m) \cdot y \cdot k \\
 a_{cyk} &= c \cdot (1-m) \cdot y \cdot k \\
 a_{myk} &= (1-c) \cdot m \cdot y \cdot k \\
 a_{cmyk} &= c \cdot m \cdot y \cdot k
 \end{aligned}$$

ACKNOWLEDGEMENT

The project has been partially supported by the Swiss National Science Foundation, grant n°200020_126757 / 1. We thank M. Herbert Janser, Wifag Maschinenfabrik, Bern, for having pointed to the necessity of performing the calibration of the spectral prediction model at run time, preferably without printing dedicated uniform color patches.

REFERENCES

- [1] R. Bala, "Device Characterization", Chapter 5 in *Digital Color Imaging Handbook*, G. Sharma, CRC Press, 2003, pp. 269-379.
- [2] D.R. Wyble, R.S. Berns. "A Critical Review of Spectral Models, Applied to Binary Color Printing," *Journal of Color Research and Application*, Vol. 25, No. 1, 2000, pp. 4-19, with the Demichel equations originally published in M.E. Demichel, *Procédé*, Vol. 26, 1924, pp. 17-21.
- [3] L.A. Taplin, R.S. Berns, "Spectral color reproduction based on a six-color inkjet output system," *Proc. IS&T/SID Ninth Color Imaging Conference*, 2001, pp. 209-213.
- [4] R. D. Hersch, F. Crété, "Improving the Yule-Nielsen modified spectral Neugebauer model by dot surface coverages depending on the ink superposition conditions," *Color Imaging X: Processing, Hardcopy, and Applications*, SPIE Vol. 5667, 2005, pp. 434-445.
- [5] Th. Bugnon, M. Brichon and R.D. Hersch, "Simplified Ink Spreading Equations for CMYK Halftone Prints," *Color Imaging XIII: Processing, Hardcopy, and Applications*, SPIE Vol. 6807, 2008, pp. 680717-1 to 680717-12.
- [6] H.E.J. Neugebauer, "Die theoretischen Grundlagen des Mehrfarbendrucks", *Zeitschrift fuer wissenschaftliche Photographie*, Vol. 36, 1937, pp. 36-73, translated by D. Wyble and A. Kraushaar in "The theoretical basis of multicolor letterpress printing," *Color Res. Appl.*, Vol. 30, 2005, pp. 323-331.
- [7] J.A.S. Viggiano, "Modeling the color of multi-colored halftones," *Proc. TAGA*, vol. 42, 1990, pp. 44-62.
- [8] H.R. Kang, "Applications of color mixing models to electronic printing," *Journal of Electronic Imaging*, Vol. 3, No. 3, 1994, pp. 276-287.

- [9] J.A.C. Yule, W.J. Nielsen, "The penetration of light into paper and its effect on halftone reproductions," *Proc. TAGA*, Vol. 3, 1951, pp. 65-76.
- [10] R. Bala, G. Sharma, V. Monga, and J. Van de Capelle, "Two-dimensional transforms for device color correction and calibration," *IEEE Trans. Image Process.*, vol. 14, 2005, pp. 1172-1186.
- [11] R. Balasubramanian, "Optimization of the spectral Neugebauer model for printer characterization," *Journal of Electronic Imaging*, Vol. 8, No. 2, 1999, pp. 156-166.
- [12] T. Ogasahara, "Verification of the Predicting Model and Characteristics of Dye-Based Ink Jet Printer," *Journal of Imaging Science and Technology*, Vol. 48, No. 2, 2004, pp. 130-137.
- [13] K. Iino, R.S. Berns, "Building color management modules using linear optimization I. Desktop," *Journal of Imaging Science and Technology*, Vol. 42, No. 1, 1998, pp. 79-94.
- [14] K. Iino, R.S. Berns, "Building color management modules using linear optimization II. Prepress system for offset printing," *Journal of Imaging Science and Technology*, Vol. 42, No. 2, 1998, pp. 99-114.
- [15] M. Xia, E. Saber, G. Sharma, A. M. Tekalp, "End-to-end color printer calibration by total least squares regression," *IEEE Trans. Image Process.*, vol. 8, 1999, pp. 700-716.
- [16] A. U. Agar and J. P. Allebach, "An Iterative Cellular YNSN Method for Color Printer Calibration," *Proc. of the 6th IS&T/SID Color Imaging Conference*, Scottsdale AZ, 1998, pp. 197-200.
- [17] R. D. Hersch, P. Emmel, F. Collaud, F. Crété, "Spectral reflection and dot surface prediction models for color halftone prints," *Journal of Electronic Imaging*, Vol. 14, No. 3, 2005, pp. 033001-12.
- [18] Th. Bugnon, M. Brichon and R.D. Hersch, "Model-Based Deduction of CMYK Surface Coverages from Visible and Infrared Spectral Measurements of Halftone Prints," *Color Imaging XII: Processing, Hardcopy, and Applications*, SPIE Vol. 6493, 2007, pp. 649310-1 to 649310-10.
- [19] R.D. Hersch, M. Brichon, T. Bugnon, M. Hébert, "Deducing ink spreading curves from reflection spectra acquired within printed color images," *Journal of Imaging Science and Technology*, Vol. 53, No.3, 2009, paper 030502, pp. 1-7.
- [20] T.F. Coleman, Y. Li, "A Reflective Newton Method for Minimizing a Quadratic Function Subject to Bounds on Some of the Variables," *SIAM Journal on Optimization*, Vol. 6, No. 4, 1996, pp. 1040-1058.
- [21] P.E. Gill, W. Murray, and M.H. Wright, "Practical Optimization," Academic Press, London, UK, 1981.
- [22] G. Sharma, "Digital Color Imaging Handbook," Chapter 1, CRC Press, 2003, pp. 35-36



Thomas Bugnon received his M.S degree in Communication Systems from the École Polytechnique Fédérale de Lausanne (EPFL), Switzerland, in 2005.

He joined the group of Prof. R. D. Hersch at the Peripheral Systems Lab in 2005 as a research assistant. After having worked on anti-counterfeiting techniques, he has been a PhD candidate since 2007. His research focuses on spectral prediction models for color reproduction.



Roger D. Hersch received the engineering and PhD degrees from ETH Zurich in 1975 and from EPFL in 1985, respectively. He is a professor of computer science and head of the Peripheral Systems Laboratory at the École Polytechnique Fédérale de Lausanne (EPFL), Switzerland.

He has published more than 100 scientific papers, is the editor of several books, and is inventor or co-inventor in many patent applications. He is interested in novel imaging techniques related to color prediction, color reproduction, artistic imaging, and security printing. He is a member of the IEEE Computer Society, and a fellow of IS&T (Society for Imaging Science and Technology).